ASTRONOMY
AND
ASTROPHYSICS

The comptonized X-ray source X 1724−308
in the globular cluster Terzan 2

M. Guainazzi[1]**, A. N. Parmar**[1]**, A. Segreto**[1,2]**, L. Stella**[3]**, D. Dal Fiume**[4]**, and T. Oosterbroek**[1]

[1] Astrophysics Division, Space Science Department of ESA, ESTEC, Postbus 299, 2200 AG Noordwijk, The Netherlands
[2] Istituto di Fisica Cosmica ed Applicazioni dell'Informatica, C.N.R., Via Ugo la Malfa 153, I-90146 Palermo, Italy
[3] Osservatorio Astronomico di Roma, Via dell'Osservatorio, I-00044 Monteporzio Catone, Italy
[4] Istituto Tecnologie e Studio delle Radiazioni Extraterrestri, C.N.R., Via Gobetti 101, I-40129 Bologna, Italy

Abstract. We report on the BeppoSAX observation of the X-ray source X 1724−308 in the globular cluster Terzan 2. The broadband spectrum can be described as the superposition of a power–law with photon spectral index $\Gamma \simeq 1.6 - 1.9$ and a thermal component with typical temperature $kT \sim 1$ keV. X 1724−308 is detected in the PDS up to 150 keV with a S/N ratio >3, notwithstanding a sharp exponential cutoff with $E_{cutoff} \simeq 90$ keV. The broadband spectrum can be best interpreted as due to the Comptonization of a Wien photon distribution with $kT_W \sim 1$ keV by a spherically-symmetric hot plasma with electron temperature $kT_e \sim 30$ keV and optical depth $\tau \simeq 3$. A comparison with the fainter and steeper state, which was observed by EXOSAT, suggests a correlation between the temperature of the Comptonizing electron distribution (or the plasma optical depth) and the X-ray intensity. The X–ray thermal component could originate from a boundary layer between the accretion disk and the compact object, or from the accretion disk itself.

Key words: X-rays: stars – globular clusters: individual: Terzan 2 stars: neutron stars: individual: X 1724−308 – binaries: close accretion, accretion disks

1. Introduction

The globular cluster Terzan 2 has been known to contain a luminous X-ray source since the late 1970s. An X-ray burst from a region including the cluster was observed by OSO-8 (Swank et al. 1977), and the same mission detected persistent emission from a location consistent with the cluster. *Uhuru* (Forman et al. 1978) and *Einstein* High Resolution Imager (HRI, Grindlay et al. 1980) observations placed this source in the core of the cluster. The source is known either as X 1724−308 (Parmar et al. 1989; hereafter P89) or 1E 1724−305. It has a rather hard (photon index $\Gamma \sim 2$) power–law spectrum, with a 1–20 keV flux which varies by about a factor of 4 ($2.5 - 10 \times 10^{-10}$ erg s^{-1} cm^{-2}). *Einstein* data suggest that in a higher flux state ($F_{1-20~keV} \simeq 2.1 \times 10^{-9}$ erg cm^{-2} s^{-1}) the source softens and the X-ray spec-

trum is better described by a $\sim$6 keV bremsstrahlung (Barret et al. 1998, in preparation).

Terzan 2 is a relatively dim globular cluster, with an estimated distance of $\sim$10 kpc and visual extinction $A_V = 4.03$, according to Djorgovski (1993). The scatter on the values reported in the literature for these quantities is however rather high ($\sim 30\%$ and $\pm^{15}_5\%$, respectively; see Ortolani et al. 1997 and references therein). The power–law intensity profile of its surface brightness and the relatively low core star density argue for a complex dynamical history (Djorgovski et al. 1986).

Terzan 2 is one of the two globular clusters from which X-ray emission was detected at energies >40 keV by *Sigma* (Barret et al. 1991). The *Sigma* source (GRS 1724−308) was observed several times between 1991 and 1994 and appears to be variable (Goldwurm et al. 1994). The 1991 detections (at a total 6.8σ confidence level) are consistent with a simple power–law spectrum with $\Gamma = 1.6^{+0.4}_{-0.6}$ and a 38–200 keV flux of $\sim$5.8 $\times$ 10^{-3} photons cm^{-2} s^{-1}, corresponding to a poorly determined 1–20 keV flux of between 1.5 and 13×10^{-10} erg cm^{-2} s^{-1}. ROSAT HRI observations by Mereghetti et al. (1995) did not reveal any other X-ray sources within $3'.5$ from the cluster core, supporting the identification of GRS 1724−308 with X 1724−308. The existence of a population a low-luminosity (*i.e.*: $\lesssim$ a few 10^{33} erg s^{-1}) sources in Terzan 2, similar to those discovered in the cores of 47 Tuc (Hasinger et al. 1994) or ω Cen (Johnston et al. 1994) cannot be excluded. The X–ray flux of these sources would be $\sim$3 orders of magnitude lower than that of X 1724−308 and their existence therefore would not affect any of the conclusions in this *paper*.

Recent RXTE observations of X 1724−308 (Olive et al. 1998) suggest that its timing properties are typical of an "atoll" source. The Power Spectrum Density (PSD) can be well modeled with the sum of two "shot noise" components, with shot decay timescales of $\sim$16 and $\sim$680 ms. A Quasi-Periodic Oscillation (QPO) feature at $\sim$0.8 Hz was also detected in the PSD. The claim of another QPO feature at $\nu \simeq 0.092$ Hz observed by the Medium Energy (ME) instrument on board EXOSAT (Belli et al. 1986) remains unconfirmed. The X-ray spectral hardness and the continuum properties of the PSD resemble those of some black hole candidates.

As part of the BeppoSAX Core Program, a number of X-ray luminous globular clusters are being observed. A discussion of the properties of the sample will be deferred to a forthcoming paper. Here, we report the results of the BeppoSAX observation of X 1724−308.

2. Observation and data reduction

Results from all the co-aligned instruments on board BeppoSAX (Boella et al. 1997a) are presented: the Low-Energy Concentrator Spectrometer (LECS; 0.1–10 keV; Parmar et al. 1997), the Medium-Energy Concentrator Spectrometer (MECS; 1.3–10 keV; Boella et al. 1997b), the High Pressure Gas Scintillation proportional Counter (HPGSPC, 4–120 keV, Manzo et al. 1997) and the Phoswich Detection System (PDS; 15–300 keV; Frontera et al. 1997). The MECS consisted at the time of the X 1724−308 observation of three identical grazing incidence telescopes with imaging gas scintillation proportional counters in their focal planes (now only two are operating). The LECS uses an identical concentrator system as the MECS, but utilizes an ultra-thin (1.25 μm) entrance window and a driftless configuration to extend the low-energy response to 0.1 keV. The fields of view (FOV) of the LECS and MECS are circular with diameters of 37′ and 56′, respectively. The non-imaging PDS consists of four independent units arranged in pairs each having a separate collimator. Each collimator can be alternatively rocked on- and off-source to monitor the background counting rate. The hexagonal PDS FOV is 78′ full-width at half maximum. The HPGSPC was similarly operating in rocking mode, but only the "off-" position has been employed to monitor the background. Several pieces of evidence indicate that there are no significant contaminating sources present in the PDS FOV, both in the "on" and in the "off" positions: the "off" count rates are in good agreement with the long–term increasing trend of instrumental background studied by Guainazzi & Matteuzzi (1997); the "on" and "off" light curves show the same variability pattern (∼20% of count rates in the whole energy bandpass), which is due to the variation of the particle background around the orbit, thus excluding the presence of a strongly variable or transient unknown source and finally the PDS spectrum aligns very well with those from the other instruments (see Sect. 3). Similar arguments apply to the HPGSPC data.

The region of sky containing X 1724−308 was observed by BeppoSAX between 1996 August 17 04:29:05 UT and August 18 05:05:11 UTC in an observation lasting 65 ks and spanning 12 orbital cycles. Good data were selected from intervals when the elevation angle above the Earth's limb was >4° and when the instrument configurations were nominal, using the SAX-DAS 1.3.0 data analysis package (Lammers 1997; custom software has been used to reduce the HPGSPC data). Additionally, PDS data within 5 minutes after each South Atlantic Anomaly passage were excluded to avoid intervals were the gain was recovering to its nominal value following switch-on. This gives exposure times of 7.3 ks, 37.1 ks, 10.5 ks and 16.7 ks for the LECS, MECS, HPGSPC, and PDS, respectively. The standard PDS (HPGSPC) collimator rocking angle of 210′ (180′), and

standard dwell time of 96 s for each on- and off-source position were used. The LECS was operated only during satellite night-time and was switched-off during the second half of the observation for technical reasons.

3. Data analysis

LECS and MECS data were extracted centered on the position of X 1724−308 using radii of 8′ and 4′ respectively, corresponding to $\simeq 95\%$ of the instrumental Point Spread Functions. Background subtraction in the imaging instruments was performed using standard files, but is not critical for such a bright source. Background subtraction in the HPGSPC and PDS was performed using data from the offset detectors. The background-subtracted count rates of X 1724−308 are $3.2\,s^{-1}$, $10.4\,s^{-1}$, $11.2\,s^{-1}$ and $6.1\,s^{-1}$ in the LECS, MECS, HPGSPC, and PDS, respectively. Spectra have been rebinned so as to have at least 30 counts per energy channel and to sample the instrumental energy resolution with no more than 3 spectral channels, in order to ensure the applicability of χ^2 fitting techniques. A systematic error of 1% has been added to each channel of the rebinned LECS and MECS spectra, to account for the residual systematic uncertainties in the detector calibration. Publicly available responses at 1997 September have been used, and spectral fits performed in the following energy ranges: 0.1–4 keV (LECS), 2.2–10.5 keV (MECS), 4–40 keV (HPGSPC), 15–200 keV (PDS). In the spectral fits, a normalization factor has been included to account for the well-known mismatch in the BeppoSAX instrument absolute flux calibration (Cusumano et al. 1998). The factors have been left completely free, except for the PDS to MECS one, which has been constrained to be in the 0.82-1.02 range (Cusumano et al. 1998). The values of the LECS to MECS and HPGSPC to MECS relative normalizations derived from the fit lie in the intervals 0.80–0.82 and 1.05–1.06, respectively. They are in good agreement with the values typically observed (0.7–1.0 and 0.8–1.05, respectively; cf. Grandi et al. 1997; Cusumano et al. 1998). Uncertainties are given at 90% confidence level for one interesting parameter, unless otherwise specified.

3.1. Timing analysis of the persistent emission

The source underwent a type I burst starting from ∼12825 s from the beginning of the observation, with an e-folding time of 25 ± 3 s. In this paper we define the "persistent" emission excluding the data from the occurrence of the burst up to the end of the next orbit. The cut corresponds to $\simeq 10^4$ s of elapsed time. Fig. 1 shows light curves of the so defined persistent emission in the 1.5–10.5 keV (MECS), 0.1–1.5 keV (LECS) and 13–200 keV (PDS) energy ranges. These energy ranges have been chosen in order to sample different spectral components (see Sect. 3.3). The χ^2 of a constant fit for these light curves is 245 for 220 degrees of freedom (dof), 96.5/62 dof and 252/210 dof, respectively. At energies $\gtrsim 1.5$ keV there is no evidence of variability, while the relatively high χ^2 obtained from the light curves at energy ≤1.5 keV is mainly due to an intensity increase of about 15% between the pre–burst and the post–burst phases.
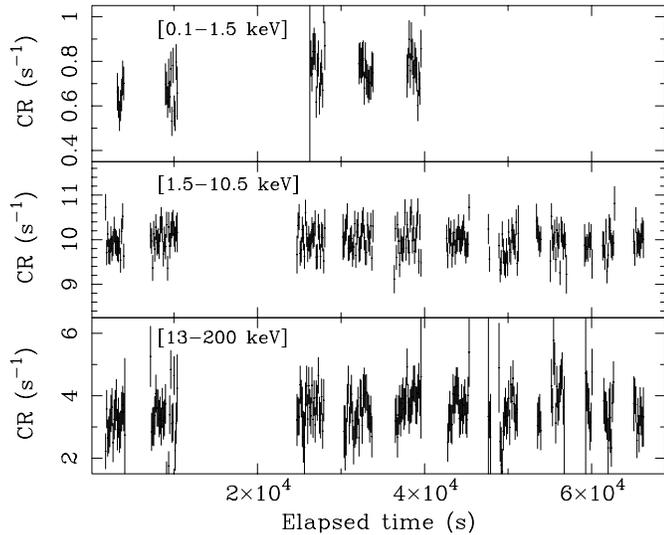
Fig. 1. Light curves in the 0.1–1.5 keV (*upper panel*), 1.5–10.5 keV (*central panel*) and 13–200 keV (*lower panel*) energy ranges. The binning time is 128 s. The LECS and MECS light curves are not background-subtracted. Only time bins with an exposure fraction $\geq 25\%$ are shown. Data from the two orbits after a Type I burst (corresponding to 12800 to 24200 s) have been removed
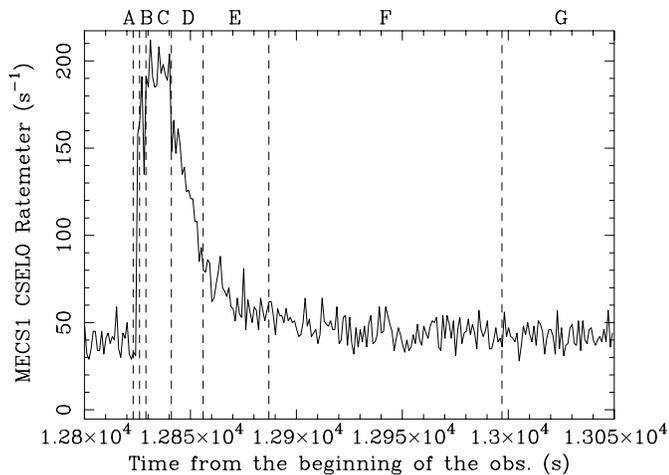

Fig. 2. Zoom of the MECS CSELO ratemeter light curve around the X1724-308 burst. Dashed vertical lines indicates the contiguous time intervals used for the time-resolved burst spectroscopy. For sake of clarity only a fraction of the "G" phase is shown, which extends for $\simeq 400$ s from t $\simeq 13000$ s

However, we will in the following analyze the time–averaged spectra of all instruments. In Sect 3.4 we show that the induced systematic uncertainties are smaller that the statistical errors on the spectral parameters, even in the simplest parameterization.

3.2. The burst

A profile of the burst in the full MECS bandpass is shown in Fig. 2. The ratemeter CSELO (which registers the total count rate above a low energy threshold) is used to preserve the con-

tinuity of the burst profile in the plot, since some of the event scientific packets at the peak of the burst were missing due to telemetry losses. The burst shows a typical exponential decay with e-folding time 25 ± 3 s. We have performed a spectral analysis of the burst in 7 contiguous time intervals (labeled as phases "A" to "G" in the following). The borders of the intervals are shown as dashed vertical lines in Fig. 2. The LECS and HPGSPC were switched off during most of the burst and PDS detection is generally too faint to allow time-resolved spectroscopy on these small time scales. Therefore, spectra of the MECS data only have been extracted, except for the phases "F" and "G", when LECS data were available. The average persistent spectrum has been used as background. Since the persistent emission in the 2–10 keV band is constant on timescales $\sim 10^2$ s within $\pm 5\%$, time-resolved burst spectra were extracted under the condition that that 2–10 keV count rate was $\gtrsim 20\%$ of the persistent one. At lower count rates, the uncertainties on the true instantaneous level of the persistent emission make the determination of the spectral parameters meaningless. The spectra have been fitted with a simple blackbody emission, photoelectrically absorbed by a column density, N_H, of neutral matter. All the parameters were allowed to vary, except the absorbing column density in the phase "C" spectral fit, which turned out to be unconstrained and was therefore fixed to the average of the best–fit values in phases "E" and "F" and "G". Best–fit parameters and results are reported in Table 1. The blackbody temperature decreases along the burst profile, as typically observed in this kind of burst. The apparent blackbody radius (obtained assuming spherical geometry) is consistent with being the same in all phases within the statistical uncertainties, except for the first ("A") and the latest ("F") phases, for which the best-fit is $\simeq 5 - 6$ km. While the value obtained in the former phase is likely to be strongly affected by the mixing of blackbodies with a rapidly changing distribution of temperatures during the sharp rise of the burst (and therefore probably unreliable), the latter could suggest a true decrease of the emitting region typical size with time; this suggestion is supported by the fact that the nominal best-fit value in phase "F" is indeed lower than between phases "B" to "E". However, better statistical quality of the data is required to confirm such a conclusion. The weighted average of the R_{bb} is $< R_{bb} >= 9.9 \pm 0.7$ km (11.6 ± 0.8 km if only phases between "B" and "F" are considered). The peak flux is $\simeq 5.0 \times 10^{-8}$ erg cm^{-2} s^{-1}, corresponding to a luminosity $\simeq 6 \times 10^{38}$ erg s^{-1}. The simple parameterization adopted yields an adequate fit for all spectra.

3.3. Spectral analysis of the persistent emission

We performed the spectral analysis of the persistent emission in several steps. First LECS/MECS and HPGSPC/PDS spectra were fitted separately with purely phenomenological models. The spectra of all detectors were then fitted simultaneously, assuming different physical scenarios.

A single component model with absorption provides a rather poor description of the LECS/MECS spectrum. Power–law, bremsstrahlung and blackbody spectral models were tried. All

Table 1. Best-fit parameters and χ^2 values when a simple photoelectric absorbed blackbody model is applied to the time-resolved spectra of the X1724-308 burst. T_{exp} is the exposure time, CR the (persistent emission subtracted) count rate in the 2–10 keV MECS bandpass, R_{bb} is the radius of a spherical blackbody emitting region and L_X the total X-ray luminosity. Errors on CR correspond to 1-σ.

Phase	T_{exp} (s)	CR (s^{-1})	N_H $10^{22}\,cm^{-2}$	kT (keV)	R_{bb} (km)	L_X $(10^{38}\,erg\,s^{-1})$	χ^2/dof
A	2.8	149 ± 8	< 6.3	$3.1\pm^{1.0}_{0.5}$	$5\pm^2_4$	$3.5\pm^{1.9}_{0.7}$	4.6/9
B	1.17	420 ± 20	< 4.0	$2.2\pm^{0.3}_{0.2}$	$13\pm^3_4$	$5.4\pm^{1.0}_{0.7}$	6.6/10
C	0.79	480 ± 20	$1.2^\dagger$	$1.93\pm^{0.20}_{0.18}$	18 ± 4	6.0 ± 0.2	5.5/8
D	3.9	250 ± 8	< 1.7	$2.1\pm^{0.3}_{0.2}$	11 ± 3	$3.1\pm^{0.4}_{0.2}$	25/20
E	31.7	78.0 ± 1.7	1.4 ± 0.5	1.36 ± 0.06	$12.5\pm^{1.2}_{1.1}$	0.69 ± 0.04	41.2/40
F	104.7	18.8 ± 0.5	$1.3\pm^{0.9}_{0.7}$	1.08 ± 0.08	$9.2\pm^{1.5}_{1.4}$	$0.151\pm^{0.016}_{0.013}$	60.3/40
G	401.9	3.22 ± 0.19	$0.8\pm^{0.8}_{0.5}$	$0.87\pm^{0.11}_{0.10}$	$5.8\pm^{1.4}_{1.5}$	0.025 ± 0.004	65.9/65

† fixed

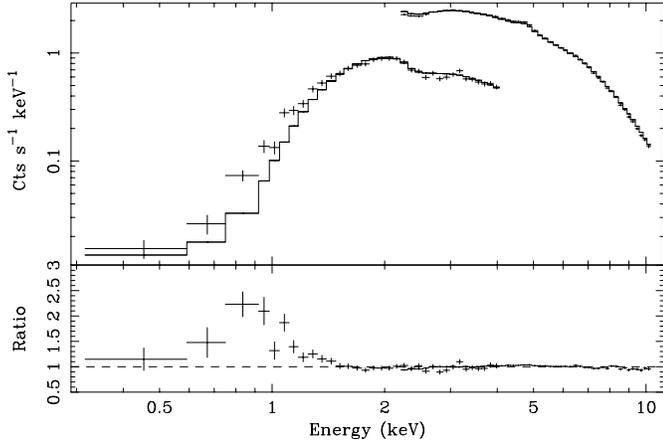**Fig. 3.** LECS and MECS spectra (*upper panel*) and data/model ratio (*lower panel*) when a photoelectric absorbed power–law is applied
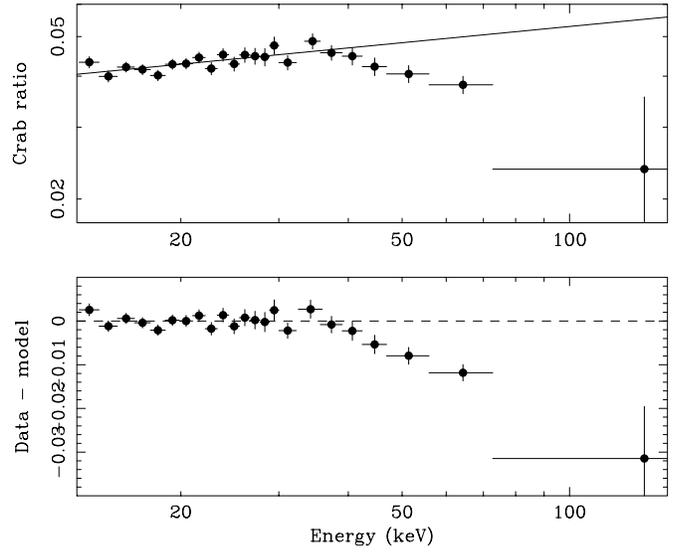

Fig. 4. Ratio of the PDS spectra of Terzan 2 and Crab (*upper panel*) and difference residuals (*lower panel*) when a power–law model is applied to fit the ratio in the 13–30 keV band and extrapolated to higher energies (*solid line*). Each data point has a S/N ratio ≥ 20

of these give large excesses above the extrapolations of the high-energy data at ~ 1 keV (see Fig. 3). A two–component model is needed to account for the observed spectrum (see Table 2). Formally, the best combination is a relatively flat ($\Gamma \simeq 1.6$) power-law + a blackbody with kT $\simeq 1$ keV. Other combinations yield a null hypothesis likelihood $\simeq 1\%$.

X 1724−308 is detected in the PDS up to $\simeq 150$ keV. One–component models give similarly poor descriptions of the HPGSPC and PDS spectra (see Table 3). There is strong evidence of a sharp roll over of the PDS spectrum above $\simeq 40$ keV (see Fig. 4). The inclusion of a cutoff in the power–law model significantly improves the quality of the fit ($\Delta\chi^2 = 129$, $\chi^2_\nu = 1.06$), yielding best-fit parameters of $\Gamma = 1.86 \pm 0.04$ and $E_{cutoff} = 90\pm^{19}_{15}$ keV. There is evidence in the HPGSPC data that the spectral index undergoes a smooth increase with energy (see Fig. 5) from $\Gamma \simeq 1.80$ at 5 keV to $\Gamma \simeq 1.90$ at 30 keV.

3.3.1. Comparing physical scenarios

Three spectral region can be phenomenologically recognized in the X 1724−308 broad-band BeppoSAX spectrum: an intermediate-hard (*i.e.*: 1.5–50 keV) power–law "emission core", with spectral index $\simeq 1.6 - 1.9$ (probably gently steepening with energy); a sharp cutoff above $\simeq 50$ keV and a soft excess at energies below $\simeq 1$ keV.

The models proposed so far to explain the X-ray emission from low-mass X-ray binaries (LMXRB) can be categorized in two main classes. The first one (originally proposed by Mitsuda et al. 1984) postulates the superposition of a multicolor blackbody emission from the inner region of an accretion disk (typical effective temperature $T_{disk} \sim 1$ keV) and of a simple blackbody originating on the surface of the neutron star ($T_{bb} \sim 2$ keV). Another class invokes unsaturated Comptonization of low-energy photons (White et al. 1985, 1986), possibly coupled with a blackbody (White et al. 1988). It has been recently suggested that these models characterize different luminosity states in LMXRB (see e.g. Tanaka 1995), the former prevailing for $L_X \gtrsim 10^{37}$ erg s^{-1}. Actually, the double blackbody scenario is ruled out by the present data, at least in its

Table 2. Best-fit parameters and χ^2 values when the models in the first column are applied simultaneously to the LECS and MECS spectra. In column 1 or in the subscripts: *wa* = photoelectric absorption; *po* = power–law; *bb* = blackbody; *brems* = thermal bremsstrahlung.

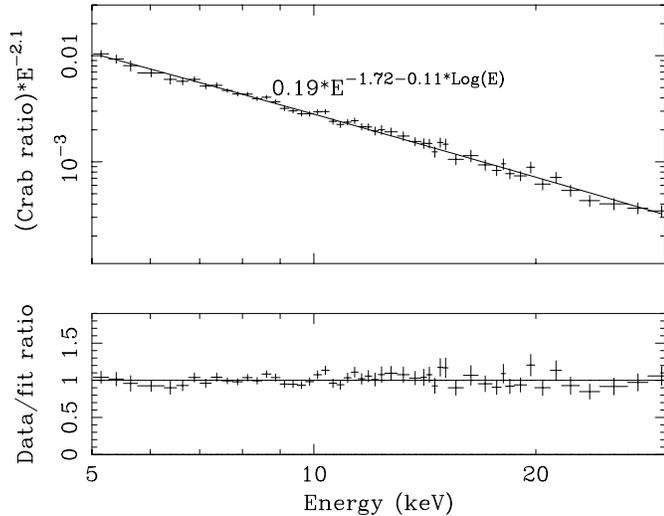| Model	N_H $(10^{22}\,\mathrm{cm}^{-2})$	Γ or kT_{brems} (keV)	T_{brems} or T_{bb} or E_{break} (keV)	χ^2/dof
wa*po	1.86 ± 0.05	$1.834\pm^{0.015}_{0.0013}$	...	303.4/76
wa*bknpo	$1.42\pm^{0.06}_{0.07}$	$1.55\pm^{0.04}_{0.06}$ $1.91\pm^{0.03}_{0.02}$	$4.3\pm^{0.3}_{0.2}$	108.4/74
wa*(po+bb)	1.31 ± 0.08	1.61 ± 0.05	$1.08\pm^{0.05}_{0.04}$	89.5/74
wa*(po+brems)	2.39 ± 0.09	1.924 ± 0.018	0.18 ± 0.02	101.6/74
wa*brems	1.38 ± 0.04	$11.6\pm^{0.2}_{0.3}$	...	123.5/76
wa*(brems+bb)	$1.46\pm^{0.06}_{0.05}$	$11.2\pm^{0.3}_{0.2}$	0.10 ± 0.03	104.0/74

Fig. 5. In the *upper panel* the ratio of the HPGSPC spectra of X1724-308 and the Crab Nebula multiplied by $E^{-2.1}$ (typical value of Crab Nebula photon index, see e.g. Cusumano et al., 1998). The solid line is the best–fit with the energy dependency law: $0.19 \times E^{-1.72-0.11\log(E)}$. The residuals in ratio between the normalized Crab ratio spectrum and the best-fit law above are shown in the *lower panel*

Table 3. Best-fit parameters and χ^2 values when the models in the first column are applied simultaneously to the HPGSPC and PDS spectra. *cutoffpl* = power–law+ cutoff.

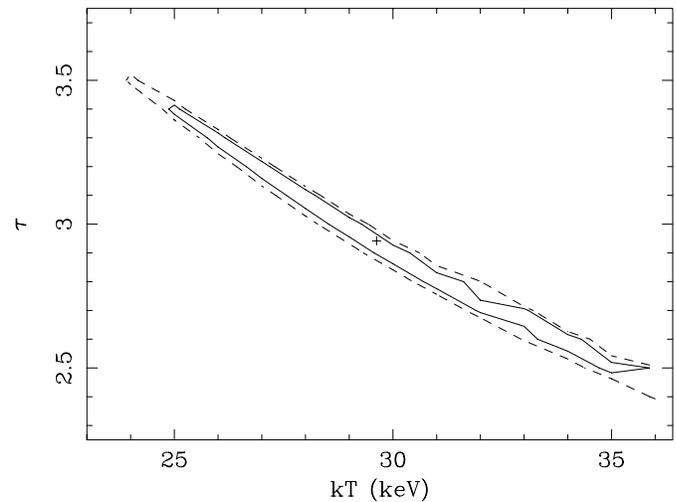| Model	Γ	kT_{br} (keV)	E_{cutoff} (keV)	χ^2/dof
po	2.104 ± 0.014	...	...	266.6/131
brems	...	$28.2\pm^{0.9}_{0.8}$	...	667.6/131
cutoffpl	1.86 ± 0.04	...	$90\pm^{19}_{15}$	137.6/130
po+brems	2.14 ± 0.08	$30\pm^{9}_{8}$	...	171.7/129

Fig. 6. Contour plot τ vs. kT_e for the model #5 in Table 4. Iso-χ^2 curves are at 90% and 99% level of confidence for two interesting parameters

simplest form. The fit with such a model yields a very poor χ^2 ($\chi^2_\nu = 21$); the proposed model does not produce enough flux at high energy to account for the relative hardness of the observed spectrum.

We have tested the viability of the Comptonization scenario with the XSPEC model compTT (Titarchuk 1994; Hua & Titarchuk 1995; Titarchuk & Lyubarskij 1995), which calculates self-consistently the spectrum produced by the Comptonization of soft photons in a hot plasma. This model contains as free parameters the temperature of the Comptonized electrons T_e, the plasma optical depth τ and the input temperature of the soft photon (Wien) distribution T_W. Both a disk and a spherical geometry for the Comptonizing plasma were tried. Again, a soft excess remains around $\simeq 1$ keV if compTT alone is applied. We have tried to model this excess either with a single temperature or with a multi temperature blackbody, for each of the two plasma geometries. The soft excess cannot instead be modeled

with a Gaussian line, even if its intrinsic width is allowed to be broad. The results are summarized in Table 4.

The above scenarios cannot be discriminated on purely statistical grounds, since the values of χ^2_ν are all very close to one. The Comptonized plasma is characterized by an electron temperature $\simeq 25$–35 keV (90% confidence level for two interesting parameters, see Fig. 6) and a geometry-independent parameters $\beta \sim 0.2$, which expresses the probability of photon scattering through the exponential factor $e^{-\beta}$ (Titarchuk 1994). The other fit parameters are slightly dependent on the assumed

Table 4. Best-fit results when Comptonization models are applied simultaneously to the LECS, MECS and PDS spectra. *diskbb* = multi-temperature accretion disk *compTT* = Comptonization. For the *compTT* model the letter in bracket indicates the disk ("d") or spherical ("s") geometry for the Comptonizing plasma. y is the Comptonization parameter ($\equiv 4[kT_e/m_ec^2]\tau^2]$) and R_W is the typical size of the input photons emitting region (following Titarchuk 1994)

#	Model	N_H $(10^{22}\,\mathrm{cm}^{-2})$	kT_e (keV)	τ	y	kT_W (keV)	R_W (km)	kT_{se} (keV)	R (km)	χ^2/dof
1	`wa*(compTT(d))`	$2.06\pm^{0.05}_{0.04}$	$24\pm^4_2$	$1.42\pm^{0.16}_{0.17}$	0.4	$0.15\pm^{0.02}_{0.03}$	350	...	...	518.6/203
2	`wa*(compTT(d)+bb)`	$0.78\pm^{0.10}_{0.07}$	$29\pm^{18}_3$	$1.17\pm^{0.17}_{0.48}$	0.3	$1.02\pm^{0.13}_{0.12}$	7.9	$0.60\pm^{0.07}_{0.06}$	$12\pm^4_3$	199.1/201
3	`wa*(compTT(d)+diskbb)`	$1.11\pm^{0.06}_{0.04}$	$28\pm^{13}_5$	$1.3\pm^{0.2}_{0.4}$	0.4	$2.10\pm^{0.18}_{0.26}$	1.8	$1.50\pm^{0.09}_{0.13}$	$2.5\pm^{0.4\dagger}_{0.2}$	194.4/201
4	`wa*(compTT(s))`	$0.48\pm^{0.04}_{0.03}$	$23\pm^4_2$	$3.7\pm^{0.3}_{0.4}$	2.5	$0.720\pm^{0.010}_{0.009}$	15	...	...	337.6/203
5	`wa*(compTT(s)+bb)`	$0.78\pm^{0.09}_{0.07}$	$30\pm^8_5$	$2.9\pm^{0.5}_{0.6}$	2.0	$1.02\pm^{0.13}_{0.10}$	8.3	$0.60\pm^{0.06}_{0.08}$	12 ± 3	198.5/201
6	`wa*(compTT(s)+diskbb)`	1.13 ± 0.04	$27\pm^{12}_4$	$3.3\pm^{0.5}_{0.7}$	2.3	$1.98\pm^{0.32}_{0.10}$	2.1	$1.44\pm^{0.16}_{0.08}$	$2.7\pm^{0.3\dagger}_{0.4}$	194.9/201

† $R = R'\cos(\theta)^{1/2}$, where θ is the inclination angle and R' is the inner radius of the disk

model used to describe the soft X-ray excess, typical values being $N_H \simeq 0.8\,(1.1) \times 10^{22}\,\mathrm{cm}^{-2}$, $kT_W \simeq 1\,(2)$ keV, $kT_{se} \simeq 0.6\,(1.5)$ keV and $R \simeq 12\,(3)$ km, when it is described with a single- (multi-) temperature blackbody. The best-fit model #5 in Table 4 superposed to the observed spectra is shown in Fig. 7. It corresponds to the following fluxes: $6.4 \times 10^{-10}\,\mathrm{erg\,cm^{-2}\,s^{-1}}$ (2–10 keV), $10.3 \times 10^{-10}\,\mathrm{erg\,cm^{-2}\,s^{-1}}$ (1–20 keV), $4.7 \times 10^{-10}\,\mathrm{erg\,cm^{-2}\,s^{-1}}$ (38–200 keV), $18.3 \times 10^{-10}\,\mathrm{erg\,cm^{-2}\,s^{-1}}$ (0.1–200 keV), the last one corresponding to an *unabsorbed* X-ray luminosity $L_X \sim 2.3 \times 10^{37}\,\mathrm{erg\,s^{-1}}$ for a distance of 10 kpc (Djorgovski 1993). Given such a continuum, the 90% upper limit on the equivalent width of a narrow line at 6.7 keV is 17 eV.

However, it must be noted that the broadband spectrum can be formally accounted by a suitable combination of three thermal models, as shown in Table 5. A bremsstrahlung with temperature $T_{br} \simeq 45 - 60$ keV is required to fit the PDS hard tail, a 0.8–1 keV blackbody can account for the soft excess, while a 1.9 keV blackbody or a $\simeq 9$ keV bremsstrahlung are needed to fill the gap between the two "extreme" spectral components. In both cases, the χ^2 is as good as for the Comptonization models.

3.3.2. The soft X-ray variability

After the burst, the 0.1–1.5 keV flux increased by $\simeq 15\%$. LECS and MECS spectra corresponding to these intervals were extracted and analyzed with the same model (model #5 in Table 4 with $kT_e = 28$ keV and $\tau = 3.1$), in order to investigate if there is any significant spectral variability associated with this flux change. The best-fit parameters are summarized in Table 6. The χ^2 for the combined fit is acceptable ($\chi^2_\nu = 1.13$). All the best-fit parameters are mutually consistent between the two intervals. We conclude that the systematic uncertainties introduced by mixing models with different normalizations are well below the statistical uncertainties, given the quality of the current data.

4. Discussion

We report on the first X-ray broadband spectrum of the burster X1724-308 in the whole 0.1–100 keV domain. The source is

detected with a S/N > 3 up to ~150 keV, confirming the previous Sigma/GRANAT results (Barret et al. 1991). The superior combination of broadband coverage, sensitivity and energy resolution has however allowed an unprecedentedly detailed spectral deconvolution, albeit formally not unique. Qualitatively the spectrum can be described as the composition of a "core", power–law emission, which undergoes a significant steepening at $E \simeq 50$ keV, and a soft excess above the extrapolation of the higher energy X-ray spectrum. The 20–200 keV flux is $\sim 3.4 \times 10^{-10}\,\mathrm{erg\,cm^{-2}\,s^{-1}}$. The corresponding luminosity at 10 kpc is $\sim 4.1 \times 10^{36}\,\mathrm{erg\,s^{-1}}$, which is typical of X-ray bursters (van Paradijs & van der Klis 1994; Barret et al. 1996).

Formally, the spectrum can be described by a suitable combination of three thermal models (models #7 and #8 in Table 5). The characterizing feature of these models is the need for a very high temperature thermal bremsstrahlung ($T_{br} \sim 50 - 60$ keV) to account for the highest energy PDS data points and cut-off roll over. The presence of such a component had already been invoked to explain the hard tail observed in several X-ray bursters (Churazov et al. 1995). The luminosity inferred by the BeppoSAX observation is $L_{br} \sim 1.4 \times 10^{37}\,\mathrm{erg\,s^{-1}}$, which implies an emission measure $< n_e V^2 > \sim 3 \times 10^{59}\,\mathrm{cm^3}$; the optically thin requirement leads to a size of a single uniform emitting cloud $>7 \times 10^{10}$ cm. Such a large region is unlikely to be directly powered by the neutron star.

The high-energy tail rules out the "double-blackbody" model (multi-temperature disk + neutron star surface), which had originally proposed by Mitsuda et al. (1984) to explain the X-ray emission of LMXRB. If a transition from a thermal- to a Comptonization-dominated hard X-ray spectrum is present in X 1724−308 (as generally believed for LMXRB), it occurs at luminosity $\gtrsim$ a few $10^{37}\,\mathrm{erg\,s^{-1}}$.

Models of the BeppoSAX spectrum of X 1724−308 which involve a Comptonized component appear therefore more plausible. A plasma with $kT_e \sim$27–30 keV and $\beta \simeq 0.2$ is required. A disk and a spherical geometry of the Comptonizing region fit the data comparably well. We note however, that somewhat higher values of the Comptonization parameter ($y \simeq 2.0$–2.3) are obtained for a spherical geometry. Similar Comptonized spec-
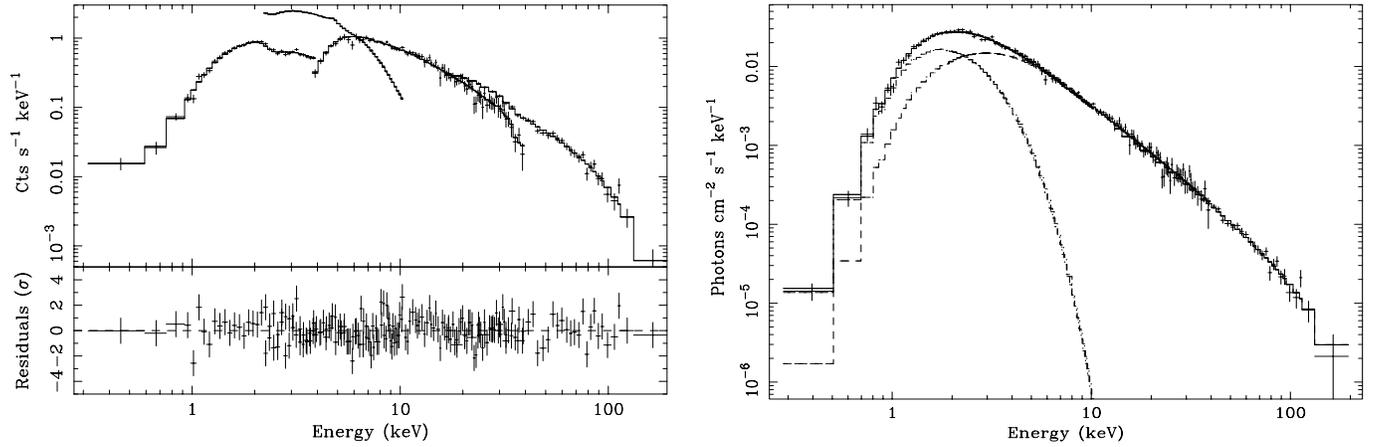
Fig. 7. *Left*: LECS, MECS, HPGSPC and PDS spectra of X 1724−308 (*upper panel*) and residuals in units of standard deviations (*lower panel*) when a the best-fit model #5 in Table 3 is applied. Each data points has a S/N ratio > 3. *Right*: the inferred photon spectrum with the best–fit model, deconvolved in the Comptonized (*dashed line*) and disk (*dot-dashed line*) blackbody components

Table 5. Best-fit results for the "thermal scenarios" of the Terzan 2 broadband spectrum. The subscripts of the kT refer to the thermal components in the model in column 1 read from the left to the right. R_{bb} is the size of a spherical optically thick blackbody emitting region

#	Model	N_H $(10^{22}\,\mathrm{cm}^{-2})$	kT_1 (keV)	R_{bb} (km)	kT_2 (keV)	kT_3 (keV)	χ^2/dof
7	wa*(bb+bb+brems)	$0.95\pm^{0.05}_{0.04}$	$0.83\pm^{0.03}_{0.04}$	$6.5\pm^{0.7}_{0.5}$ $1.17\pm^{0.16}_{0.19}$	$1.98\pm^{0.16}_{0.13}$	48 ± 3	212.3/201
8	wa*(bb+brems+brems)	$1.25\pm^{0.07}_{0.05}$	$0.99\pm^{0.05}_{0.04}$	$2.8\pm^{0.4}_{0.5}$	$9.3\pm^{1.5}_{1.3}$	$62\pm^{9}_{7}$	202.2/201

Table 6. Best–fit parameters for the joint fit of the LECS and MECS spectra extracted before and after the burst

Temporal phase	N_H $(10^{22}\,\mathrm{cm}^{-2})$	kT_W (keV)	kT_{bb} (keV)	N_{bb} $(10^{-3}\mathrm{L}_{39\mathrm{ergs}^{-1}}\mathrm{D}^{-2}_{10\mathrm{kpc}})$
Before the burst	$087\pm^{0.17}_{0.13}$	1.1 ± 0.2	$0.64\pm^{0.10}_{0.14}$	$2.6\pm^{0.9}_{1.1}$
After the burst	$0.84\pm^{0.12}_{0.09}$	$0.99\pm^{0.13}_{0.11}$	$0.57\pm^{0.07}_{0.06}$	2.3 ± 0.5

tral components have been observed in a variety of neutron star LMXRBs, although in most cases the spectra are substantially softer and the inferred electron temperatures in the 2–4 keV range (White et al. 1988). In a few Atoll sources, however, X-ray spectra extending up to ∼100 keV or more have been revealed through *Sigma*/GRANAT (Mandrou et al. 1994) and BeppoSAX (Church et al. 1998b) observations. These spectra have a clear resemblance to the spectrum of X 1724−308 discussed here, and require comparably high electron temperatures. It has also to be considered that hard tails extending to hundreds of keV are no longer believed to be exclusive to black hole candidates, at least when the LMXRB luminosity does not exceeds ∼10^{37} erg s^{-1} (Barret et al. 1994; van Paradijs & van der Klis 1994).

In the Beppo-SAX observation of X 1724−308 an additional soft spectral component is needed to fit the low energy spectrum. However, the quality of the data does not allow different models for this component to be discriminated. We find that a multi-temperature blackbody disk model, or a simple blackbody spectrum provide acceptable fits.

In the case of a multi-temperature blackbody disk model, both the derived temperature (∼2 keV) and radius of the innermost disk region (∼$3/(\cos\theta)^{1/2}$ km) are close to those obtained for the "seed" Wien spectrum for the Comptonized component (see e.g. the model #6 in Table 5). An inclination angle of ∼ 70° would be required for the inner radius of the disk to accommodate a neutron star. On the contrary the absence of a sizeable orbital modulation of the X-ray flux (absorption dips in particular) suggests a substantially lower inclination (P89; Olive et al. 1998).

If the soft thermal emission of Terzan 2 is interpreted in terms of a single temperature blackbody, the inferred linear size of the emitting region (≃ 12 km) is in good agreement with a typical neutron star and with the size inferred from the analysis of the type I burst occurred during the BeppoSAX observation. It is worth emphasizing the (single) blackbody temperature of Terzan 2 (kT∼ 0.6 keV) is a factor of 2-3 lower than that derived from most other neutron LMXRBs (cf. White et al. 1988). In the single temperature blackbody scenario, the parameters also are

close to those derived for the input spectrum to the Comptonized component, such that the neutron stellar surface might represent the source of "seed" photons. Alternatively, the analogy with the hard spectra of black hole candidates (where, of course, there is no star surface or boundary layer) suggest that even in disks around accreting neutron stars there is a hot Comptonizing plasma that coexists with a dense cold phase responsible for the generation of the "seed" photons (cf. Eardley & Lightman 1975; Galeev et al. 1979; Molendi & Maraschi 1990).

The two spectral decompositions discussed above differ a great deal in the physical interpretation of the two spectral components. In the former case the Comptonized hard component originates from the boundary layer close to the neutron star surface, whereas the soft component is produced by the sum of blackbody spectra emitted by the accretion disk. In the latter case the (single) blackbody spectrum likely arises from the boundary layer close to the neutron star surface, while the accretion disk gives rise to the Comptonized spectrum. Simple accretion disk theory predicts that, unless the neutron star is rotating very close to its break up velocity, the ratio of the accretion luminosity released in the disk to that released in the boundary layer should be equal to 1. Sunyaev & Shakura (1986) show that this ratio can be as low as ~ 0.45 if the accretion disk ends at the marginally stable orbit and this, in turn, is larger then the neutron star radius. Recent observations of fast quasi periodic oscillations, QPOs, in LMXRBs testify that the neutron stars contained in them rotate much slower than break up (periods in the $\sim$3 ms range), and that the inner radius of the accretion disk (as inferred from the frequency of the higher kHz QPO power spectrum peak) is often larger than the marginally stable orbit. This would further decrease the predicted ratio of disk and boundary layer luminosity. The 0.1–100 keV luminosities of the disk (multi-) blackbody component and the (boundary layer) Comptonized component inferred from the BeppoSAX spectrum of Terzan 2 are $\sim$$8.5 \times 10^{36}$ erg s^{-1} and $\sim 1.5 \times 10^{37}$ erg s^{-1}. The derived ratio of $\sim$0.55 is in agreement with the predictions above. However, observations of dips in several X-ray can be convincingly explained if the Comptonized component is extended (Church & Balucińska-Church 1995; Church et al. 1998a), almost at odds with the former interpretation.

In the latter interpretation the ratio of the luminosity of the Comptonized (disk) spectrum (1.9×10^{37} erg s^{-1}) and the luminosity of the (boundary layer) single temperature blackbody (2.4×10^{36} erg s^{-1}) is ~ 8, i.e. much higher then expected. An anomalously high ratio of the two components has also been found in a number of other neutron star LMXRBs (see White et al. 1988). Obscuration by an inner accretion corona or a thickened disk could decrease the relative strength of the boundary layer contribution (Lamb 1986; van der Klis et al. 1987). In the standard Shakura-Sunyaev disk, the inner radiation pressure-dominated disk can be as thick as $\sim$ few tens of kilometers, and the effect of thermal and/or secular instabilities can further enlarge it (Shakura & Sunyaev 1973; Pringle 1981). Radiation from the boundary layer might be partly scattered out of the polar channel or attenuated through a not completely optically-thick disk. A "bloated-disk" geometry has already been proposed to
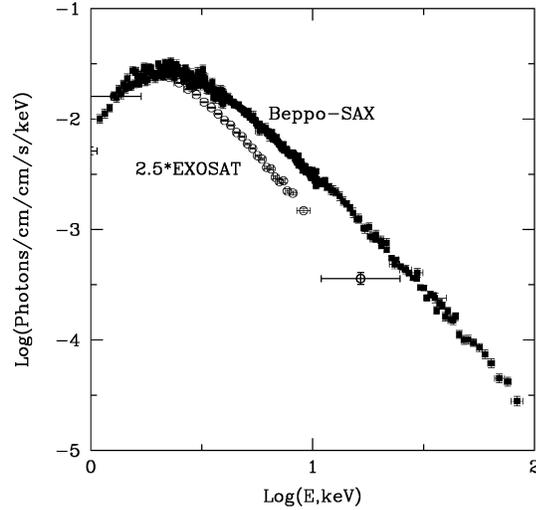

Fig. 8. Beppo-SAX and EXOSAT count spectra. EXOSAT data point have been multiplied by 2.5 to align the spectra below the photoelectric absorption cut-off

explain the low frequency QPOs observed in several LMXRBs (e.g.: 4U1820-30, Stella et al. 1987), and would be in line with the likely low inclination of the system, as inferred from the lack of significant intensity eclipses. Alternatively, exchange of energy between the magnetosphere and the accretion disk via material torque from the accretion matter could reduce the luminosity available at the surface of a neutron star, spinning at a rate close to the inner disk Keplerian frequency (Priedhorsky 1986).

The optical reddening is $A_V = 4.03$ (Djorgovski 1993). If we convert the visual absorption in an X-ray absorbing column density with $N_H = 1.8 \times 10^{21} A_V$ cm^{-2} (Predehl & Schmitt 1995), the corresponding column density is roughly consistent with the Galactic one along the line of sight to Terzan 2 ($N_{H_{Gal}} = 6.5 \times 10^{21}$ cm^{-2}, Dickey & Lockman 1990). However, the BeppoSAX observation requires a 20-75% excess absorption (depending on the spectral descriptions), in agreement with previous estimates, although rather poorly constrained and model dependent (P89; Mereghetti et al. 1995; Verbunt et al. 1995).

EXOSAT observed X 1724−308 in a factor $\sim$5 fainter and in a much softer state than BeppoSAX. This is shown in Fig. 8, where the photon spectra observed by BeppoSAX and EXOSAT are compared. The hardness difference can be parameterized as a $\Delta\Gamma \simeq 0.7$ between the observed power law photon indices. If the electron temperature remains the same, $\beta \sim 0.3$ and therefore a $\sim$50% smaller τ (Hua & Titarchuk 1995) at the EXOSAT epoch is implied (we note however that in this regime the analytical approximations on which the Comptonization Monte-Carlo simulation by Titarchuk (1994) are no longer valid and therefore the condition that T_e and β determines univocally the spectral index is not fulfilled, Hua & Titarchuk 1995). Alternatively, a steeper spectrum could imply a lower kT_e and therefore a spectral cut-off at lower energy. To check this possibility, we extracted from the public archive and re-analyzed the EXOSAT

ME spectrum of P89. A simple absorbed power–law model gives a reasonable fit ($\chi^2_\nu = 77/61$ dof), with best-fit parameters as in P89. However, the inclusion of a cut-off results in a reduction in χ^2 of 8 which is significant at 98.9% confidence. The best-fit parameters are then $N_H = (1.5 \pm 0.2) \times 10^{22}$ cm^{-2} (very similar to the BeppoSAX value in model #6 here), $\Gamma = 2.0 \pm 0.2$ and $E_{cut-off} = 14^{+21}_{-6}$ keV. We caution that this cut-off energy is very close to the upper energy range of the ME detector. If the EXOSAT result is correct, then an explanation of the difference in the two spectra may be a factor $\simeq 4$ lower electron temperature during the EXOSAT epoch. In such a scenario the energy of the electrons is physically linked with the high-energy intensity.

References

Barret D., Vedrenne G., 1994, ApJSS 92, 505
Barret D., Mereghetti S., Roques J.P., et al., 1991, ApJ 379, L21
Barret D., McClintock J.E., Grindlay J.E., 1996, ApJ 473, 963
Belli B.M., D'Antona F., Molteni D., Morini M., 1986, IAU Circ. 4174
Boella G., Perola G.C., Scarsi L., 1997a, A&AS 122, 299
Boella G., Chiappetti L., Conti G., et al., 1997b, A&AS 122, 372
Church M.J., Balucińska-Church M., 1995, A&A 300, 441
Church M.J., Balucińska-Church M., Dotani T., Asai K., 1998a, ApJ, in press (available at astroph/9805043)
Church M.J., Parmar A.N., Balucińska-Church M., et al., 1998b, A&A, in press (available at astroph/9806223)
Churazov E., Gilfanov M., Sunyaev R., 1995, ApJ 443, 341
Cusumano G., Mineo T., Guainazzi M., et al., 1998, A&A, submitted
Dickey J.M., Lockman F.J., 1990, ARA&A 28, 215
Djorgovski S., 1986, in "Instrumentation and Research Programmes for Small telescopes", IAU Symp. no. 118, Hearnshaw J.B. & Cottrel P.L. eds (Dordrecht:Reidel), p.281
Djorgovski S., 1993, in "Structure and Dynamics of the Globular Clusters", Djorgovski S. & Meylan C. eds. (S.Francisco:ASP), pag. 373
Eardley D.M., Lightman A.P., 1975, ApJ 200, 187
Forman W., Jones C., Cominsky L., et al., 1978, ApJS 38, 357
Frontera F., Costa E., Dal Fiume D., et al., 1997, A&AS 122, 357
Galeev A.A., Rosner R., Vaiana G.S., 1979, ApJ 229, 318
Goldwurm A., Cordier B., Paul J., et al., 1994, in the API Conference Proceedings n.304, "The Second Compton Symposium", eds. Fichtel C.E., Gehrels N., Norris J.P. (New York:AIP), p.421
Grandi P., Guainazzi M., Mineo T., et al., 1997, A&A 325, 17
Grindlay J.E., Marshall H.L., Hertz P., 1980, ApJ 240, L21
Guainazzi M., Matteuzzi A., 1997, BeppoSAX SDC technical Report TR-011
Hasinger G., Johnston H.M., Verbunt F., 1994, A&A 288, 466
Hua X.-M., Titarchuk L., 1995, ApJ 449, 188
Johnston H.M., Verbunt F., Hasinger G., 1994, A&A 289, 763
Lammers U., 1997, The SAX/LECS Data Analysis System Software User Manual, ESA/SSD, SAX/LEDA/0010
Lamb F.K., 1986, in "The Evolution of X-Ray Binaries", Trümper J., Lewin W.H.G. & Brinkmann W. eds. (Dordrecht:Reidel), pag. 151
Mandrou P., Roques J.P., Bouchet L., et al., 1994, ApJS 92, 343
Manzo G., Giarrusso S., Santangelo A., 1997, A&AS 122, 341
Mereghetti S., Barret D., Stella L. et al., 1995, A&A 302, 713
Mitsuda K., Inoue H., Koyama K., et al., 1984, PASJ 36, 741
Molendi S., Maraschi L., 1990, ApJ 353, 452
Olive J.F., Barret D., Boirin L., et al., 1998, A&A 333, 942
Ortolani S., Bica E., Barbuy B., 1997, A&A 326, 614
Parmar A.N., Martin D.D.E., Bavdaz M., et al., 1997, A&AS 122, 309
Parmar A.N., Stella L., Giommi P., 1989, A&A 222, 96 (P89)
Predehl P., Schmitt J.H.M.M., 1995, A&A 293, 889
Priedhorsky W, 1986, ApJ 306, L97
Pringle J.E., 1981, ARA&A 19, 137
Shakura N.I., Sunyaev R.A., 1973, A&A 24, 337
Titarchuk L., Lyubarskij Y., 1995, ApJ 450, 876
Verbunt F., Bunk W., Hasinger G., Johnston H.M., 1995, A&A 300, 732
van der Klis M., Stella L., White N., Jansen F., Parmar A.N., 1987, ApJ 316, 411
van Paradijs J., van der Klis M., 1994, A&A 281, 17
White N.E., Peacock A., Taylor B.G., 1985, ApJ 296, 475
White N.E., Peacock A., Hasinger G., et al., 1986, MNRAS 218, 129
White N.E., Stella L., Parmar A.N., 1988, ApJ 324, 363